Intergrain forces in low-Mach-number plasma wakes

I. H. Hutchinson

Plasma Science and Fusion Center and Department of Nuclear Science and Engineering, Massachusetts Institute of Technology, Cambridge, Massachusetts 02139, USA

(Received 24 April 2012; published 28 June 2012)

Large-scale particle-in-cell calculations of the plasma wake interactions of two negatively charged grains smaller than the Debye length are carried out using the COPTIC code over a wide range of subsonic plasma flow velocities. In plasmas with the temperature ratio $T_e/T_i = 100$, it is found that a single grain's oscillatory wake disappears for flow Mach numbers M less than approximately 0.3, which is the parameter regime where Landau damping is expected to be strong. Neutral collisions suppress potential oscillations above $M = 0.3$, but not the trailing attractive potential peak caused by ion focusing. The transverse (grain-aligning) force on a downstream particle in the wake of another is obtained rigorously from the code in three-dimensional simulations. It shows general agreement with the force that would be deduced from the single-grain wake potential gradient. Except for relatively large grains in the nonlinear collisional regime, the grain-aligning force is very small for slow flow.

DOI: 10.1103/PhysRevE.85.066409 PACS number(s): 52.30.−q, 52.27.Lw, 52.35.Fp, 52.20.−j

I. INTRODUCTION

The wake formed by plasma flow past a charged object is a phenomenon important for solar-system plasma physics [1], space-craft interactions [2], and understanding Langmuir probes [3,4]. It also controls the effective intergrain interaction in dusty plasmas; thus the objects embedded in the plasma will for consistency be called grains in this paper. The force between grains in flowing plasmas is known to be anisotropic and nonreciprocal. This character arises from the effect of the wake of one upon the other. It is widely found, for example, that grains suspended by the balance of forces in a plasma sheath edge often align themselves vertically [5–12] because the downstream grain experiences an attraction toward the flow axis of the upstream grain's wake. The attraction arises from focusing of ions (attracted by the negatively charged grain) enhancing the ion density in the immediate downstream region. The flow velocity in these situations is approximately equal to the sound speed.

Linear response formalism [13] has long been used to calculate the anticipated form of the wake potential of a single point charge (grain) [14–16]. Dust grains in many experiments have large enough charge, however, that they are not well represented by a linearized calculation. Early nonlinear calculations based upon fluid plasma representations (e.g., Refs. [17,18]) omit kinetic phenomena, such as ion orbit crossing and Landau damping, that are crucial to the physics. Recent kinetic collisionless particle-in-cell calculations [19] agree with linear response calculations in the linear regime, but have shown that the nonlinearities substantially suppress the wake amplitude at experimental parameters. They also have confirmed [20] (contradicting some prior claims) that the intergrain force for sonic flow is fairly well represented by the gradient of the single-grain wake potential acting on the charge of the downstream grain. As the flow velocity is reduced below the sound speed, the oscillatory wake does not immediately disappear. Nevertheless, it must eventually disappear and revert to the spherically symmetric behavior of a zero-flow situation. The question then arises as to where and how this transition takes place.

Experiments on dusty plasmas in microgravity conditions (e.g., Ref. [21]) have shown that there appears to be a mechanism aligning chains of grains far from the sheath. Recent analysis indicates that this alignment occurs in situations where the ion flow velocity is much smaller (by a factor of 10 or more) than the sound speed [22]. These observations give extra incentive to explore the behavior of the wake in low-Mach-number flows. That is the purpose of the present computational investigations.

II. CODE DESCRIPTION

The present results are obtained with the Cartesian mesh, oblique boundary, particles and thermals in cell (COPTIC) code. It is a hybrid particle-in-cell code in which the electron density is presumed governed by a simple thermal Boltzmann factor $n_e = n_{e\infty}\exp(\phi e/T_e)$. The ions are represented by particles moving according Newton's second law under the influence of the self-consistently calculated electrostatic potential ϕ. Objects of various shapes can be embedded in the three-dimensional Cartesian computational mesh and their boundaries are treated with second-order accuracy by the finite-difference scheme even if their surfaces are oblique to the mesh [23]. In addition, infinitesimal point-charge grains can be included using a particle-particle–particle-mesh [24] scheme. In the present work, only point grains are included. Prior studies have shown that such calculations are fully representative of grains with a radius up to one-tenth of the Debye length ($r_p \leqslant 0.1\lambda_{\rm De}$, where $\lambda_{\rm De}^2 = \epsilon_0 T_e/n_e e^2$). A fuller description of COPTIC has already been published [19].

In the present work, calculations have been performed with and without charge-exchange collisions. The collision implementation is the same as for the SCEPTIC code [25], consisting of Poisson statistically distributed collisions with a fixed (velocity-independent) collision frequency (inverse of collision time). After the collision the ion acquires a new velocity distributed according to the supposed neutral distribution function, which is taken to be a Maxwellian shifted by the same flow velocity as the external ion drift. In this situation no external field is required to sustain the drift and

the external ion distribution is the same shifted Maxwellian. Its temperature is $T_i = T_e/100$, which is appropriate for approximately room temperature ions in a partially ionized plasma. The external drift velocity v_d is in the direction $\hat{\mathbf{z}}$ and is expressed as a Mach number by dividing the velocity by the cold-ion sound speed $c_s = \sqrt{T_e/m_i}$: $M = v_d/c_s$.

Ions are continuously injected at the boundary at a rate and with a distribution corresponding to the external plasma density, temperature, and flow. Ions are removed from the simulation when they leave the computational box. Poisson's equation for the potential is solved for each time step with the charge density determined by the self-consistent electron and ion densities, assigned by the so-called cloud-in-cell [26] algorithm to the finite-difference lattice. The code is advanced in time by a leapfrog scheme until it converges to a steady state. The boundary conditions on Poisson's equation at the edge of the computational mesh are designed to model a perturbed region within a wider unperturbed background. On the leading edge, the normal potential gradient is set to zero. On the sides of the box, to which the external drift is tangential, the potential gradient is set to zero in the direction $M\hat{\mathbf{z}} + \hat{\mathbf{r}}$, where $\hat{\mathbf{r}}$ is the direction of the cylindrical radius $r = \sqrt{x^2 + y^2}$. This oblique choice acts approximately as a nonreflecting boundary condition for the oblique perturbations of the wake. At the trailing face, the potential boundary condition is equivalent to $\partial^2\phi/\partial z^2 = -\phi/(M\lambda_{\mathrm{De}})^2$, which is nonreflecting for the dominant wavelength of perturbation. These choices minimize the effects of the boundary proximity on the potential solution in the inner region and hence allow a relatively compact computational domain without significant boundary effects, as has been confirmed by trials with a larger box.

The force on a grain is obtained by surrounding it by a sphere across which the momentum flux of ions, electrons, and fields (i.e., the Maxwell stress) is accumulated. When collisions are present, they give rise to a bulk momentum source (or sink) within the sphere's volume that must also be accounted for. The way in which this is done has been explained elsewhere [27]. Then in steady state, the value obtained for the total momentum flux to the grain ought to be independent of the size of the sphere—and it is.

The calculations presented here are for nominally point grains, which are known from previous simulations [19] to give results very similar to finite-size small grains. However, especially for the collisional cases included here, the code actually behaves as if a small absorbing object were present at the point. Ions that happen to step very close to the point charge experience an extremely large acceleration (which is evaluated directly in terms of Coulomb force). The impulse they acquire in a single time step can then be sufficient to impart (unphysically) a high velocity sufficient to move them directly out of the mesh on the next step. Thus they are removed from the simulation, effectively as if they were absorbed when approaching the grain too closely. For force calculations it is preferable simply to drop them from the simulation when their single-step impulse exceeds $5m_ic_s$ rather than accumulating their big unphysical momentum impulse that enhances the noise level of the force measurement. The removal of ions is thus equivalent to the presence of an absorbing grain whose radius depends upon grain charge and time-step duration. For the parameters used here, this effective radius does not exceed approximately $0.02\lambda_{\mathrm{De}}$.

A time step of 0.025 is used in the simulations. It is equal to the distance (in Debye lengths) traveled in one step at the sound speed. Therefore, orbits closer to the charges than approximately this distance are incorrectly integrated at the standard time step. A scheme of automatic refinement of the time step is used for the cases plotted. It keeps the per-substep impulse below $2m_ic_s$ by taking multiple substeps shorter than the standard step by a factor up to 8. This accuracy improvement reduces the ion loss caused by an excessive single-step impulse, but does not affect substantially the results other than reducing the noise. The resulting ion self-force is negligible.

Calculations are performed in dimensionless units. The lengths reported here are all normalized to the Debye length λ_{De}, in figure labeling sometimes abbreviated as λ.

III. SINGLE-GRAIN WAKE

At sonic ion flow speeds, it has been shown by two-grain simulations with COPTIC [20] that the transverse force on a grain in the collisionless wake of another is well approximated as being given by the gradient of the potential of the wake of the upstream grain in the absence of the downstream grain, acting on the downstream grain's charge. In other words, the force on the downstream grain can be derived directly from the upstream grain's unperturbed wake field. Although this identity has not been previously established for deeply subsonic flow speeds, it suggests that we should first examine what happens to the single-grain wake potential as the Mach number is decreased. Prior calculations of the wake potential (e.g., Refs. [28,29]) have rarely if ever systematically explored values less than $M = 0.5$, but linear response calculations are being pursued [30].

Shown in Fig. 1 are contour plots of the wake potential of a single grain. These are in principle rotationally symmetric, i.e., functions of only r and z, so they are obtained by averaging the three-dimensional solutions of COPTIC over the cylindrical angle θ. (This gives a total r extent up to $\sqrt{2}$ times the box half-width, but values beyond that half-width of 4 become increasingly subject to distortion by the boundary proximity.) Figure 1(a) gives the result for $M = 0.6$, plotting also the mirror image (at negative r) to emphasize the conical structure of the wake oscillations. Figures 1(b) and 1(c) show only the positive half, for $M = 0.4$ and 0.2 respectively, using the same contour values. By the time the Mach number has been lowered to 0.2 all the oscillations in the wake have vanished and one is left with simply the potential well of the negatively charged grain.

Shown in Figs. 2 and 3 are potential profiles along the axis of the simulation ($x = 0$, $y = 0$). The value of normalized grain charge $\bar{Q} \equiv Q/(4\pi\epsilon_0\lambda_{\mathrm{De}}T_e/e)$ (where Q is the unnormalized grain charge) determines the strength of the interaction. For grains small compared with λ_{De} (the situation considered here), $\bar{Q} \approx (e\phi_p/T_e)(r_p/\lambda_{\mathrm{De}})$, where ϕ_p is the grain's surface potential. An isolated grain floats at a surface potential of approximately $-2T_e/e$; therefore $\bar{Q}$ can be considered to represent the size of the grain relative to

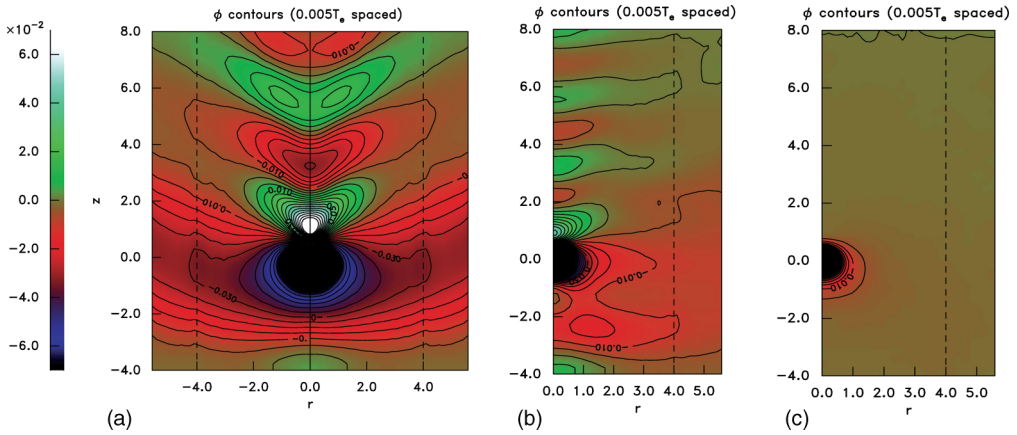

FIG. 1. (Color online) Wake potential contours for a single grain. (a) $M = 0.6$, (b) $M = 0.4$, and (c) $M = 0.2$. In the collisionless plasma, nonlinear regime the point charge $\bar{Q} = -0.2$.

the Debye length: $r_p \approx \lambda_{De}|\bar{Q}|/2$. When the charge is small $\bar{Q} = -0.02$, as in Fig. 2, prior investigations have shown the response to be nearly linear and to agree with linear response formalism [19]; however, when it is ten times larger $\bar{Q} = -0.2$, as in Fig. 3, there are already strong nonlinear modifications of the response even for sonic flow. Slower flow velocities, such as those we are investigating here, are expected to experience stronger nonlinearities than in prior calculations. The modification is predominantly a suppression of the magnitude of the oscillatory potential in the wake. This shows up when comparing Figs. 2 and 3 in that the wake potential peak normalized to $\bar{Q}$ is approximately three times smaller for the nonlinear case than for the nearly linear case. (Exact linearity would give equal normalized potentials $\phi/\bar{Q}$.) We also compare (a) collisionless plasmas with (b) plasmas in which substantial ion-neutral charge-exchange collisions occur. Many experiments have sufficient background neutral pressure for collisions to be important. The collision time chosen here is $\tau = 1.3\lambda_{De}/c_s$, giving rise to a collision length of approximately λ_{De} for ions at the sound speed. This collisionality is a reasonable approximation for Debye lengths somewhat less than a millimeter in argon gas of pressure a few tens of Pa, which is typical of some experimental conditions. (However, it is not intended to model experimental collision effects precisely since the physical collision frequency is not independent of ion velocity.)

As the Mach number is decreased, for the collisionless plasma, the wavelength of the potential oscillations in the collisionless wake continues to be rather well given by the expression $2\pi\lambda_{De}M$ established for transonic flow. This value can be understood qualitatively as a radial compressional ion oscillation of frequency ω_{pi} (induced by the presence of the grain) convected by the flow at speed Mc_s. The oscillations persist for $M \geqslant 0.4$ but disappear rather abruptly for smaller drift velocity. In these plasmas with $T_i/T_e = 0.01$, the ion thermal velocity is $\sqrt{T_i/m_i} = 0.1c_s$. Therefore, the disappearance of the oscillations at $M = 0.3$ (and below) occurs where linear Landau damping becomes strong, conventionally considered to be at a phase velocity three times the thermal velocity.

This interpretation is supported by other COPTIC calculations (not shown here) at a temperature ratio $T_i/T_e = 0.1$, which show wake oscillations disappearing below approximately $M = 0.8$ (2.5 times the thermal velocity). The trailing

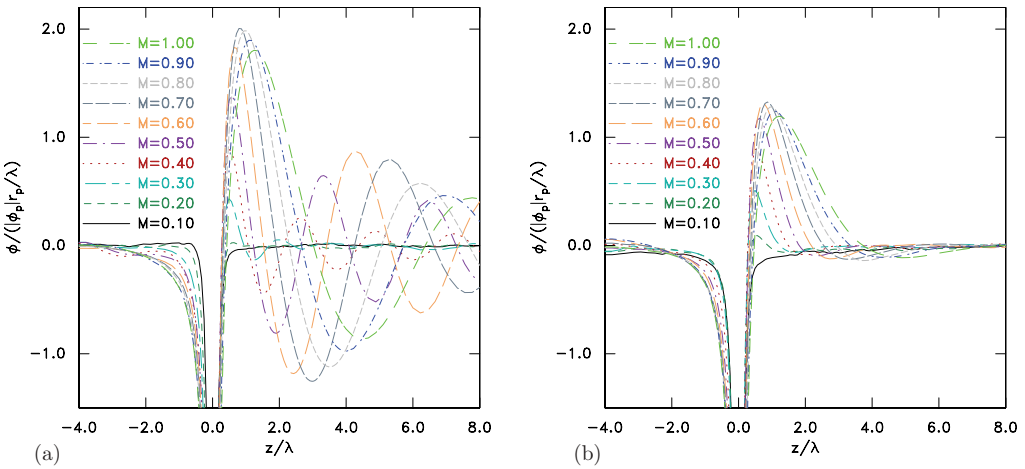

FIG. 2. (Color online) Wake axial potential profile for Mach numbers M. In the nearly linear regime the point charge $\bar{Q} = -0.02$. (a) Collisionless plasma and (b) collisional plasma (collision time $1.3\lambda_{De}/c_s$).

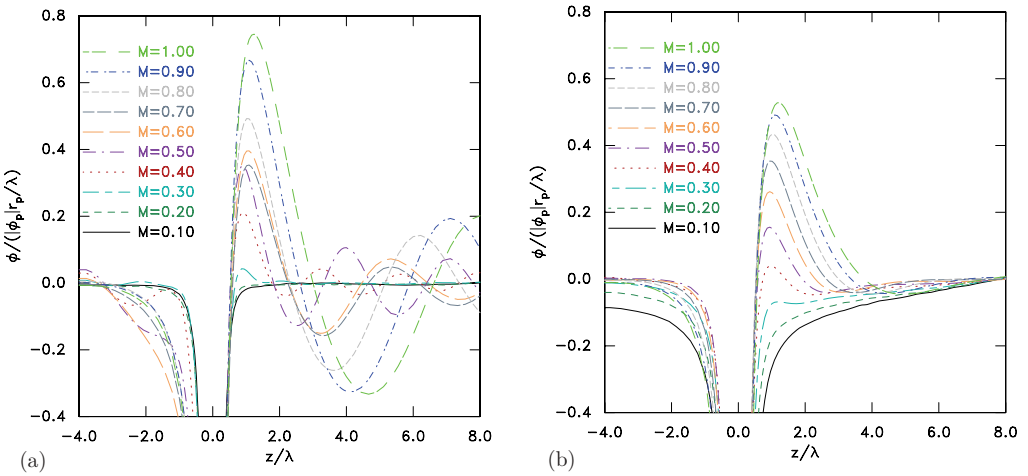

FIG. 3. (Color online) Wake axial potential profile for Mach numbers M. In the nonlinear regime the point charge $\bar{Q} = -0.2$. (a) Collisionless plasma and (b) collisional plasma (collision time $1.3\lambda_{De}/c_s$).

potential peak then disappears below approximately $M = 0.5$, suggesting that it is less susceptible to Landau damping *per se*.

Substantial charge-exchange collisionality, when the collision time equals $1.3\lambda_{De}/c_s$, has the effect of suppressing the oscillatory wake. However, collisionality does not remove the large positive potential peak that immediately follows the grain. It only reduces its height by up to 40%. That peak is attractive to other negatively charged grains and is considered the cause of vertical alignment of pairs of grains suspended in a sheath edge.

This trailing attractive potential region disappears for both collisional and collisionless plasmas when M decreases. A vestige is left when $M = 0.3$, which essentially vanishes for $M \leqslant 0.2$. It is interesting to notice that this transition coincides with the filling in of the potential depression at the *upstream* side of the grain (most noticeable for collisionless plasmas). This leading potential well has a scale length of at least λ_{De} for $M > 0.4$, but it fills in, yielding an upstream scale length much shorter for slower drifts. This is presumably a reversion from electron shielding to ion shielding, the ion Debye length here being ten times shorter than λ_{De}.

Potential profiles in the direction transverse to the flow determine the transverse electric field, which gives a force tending to align the grains. Examples are shown in Figs. 4 and 5 at a distance downstream of one Debye length ($z = 1\lambda_{De}$, $y = 0$). We observe the rapid transition from an attractive (positive) potential to a practically flat potential as M drops below 0.4. Actually, in collisional cases, the potential becomes slightly negative (repelling) at the lowest values of M.

The reason for the presence of the extended potential well in collisional plasmas, which is most obvious in the nonlinear case [Figs. 3(b) and 5(b)], is that the effective absorption of ions at the grain causes an inflow of ions. Its magnitude is controlled effectively by the collision rate and prescribed large grain charge (and not by the somewhat ill-defined effective computational grain size). This inflow, which is illustrated in Fig. 6, becomes the dominant effect on the potential profile at

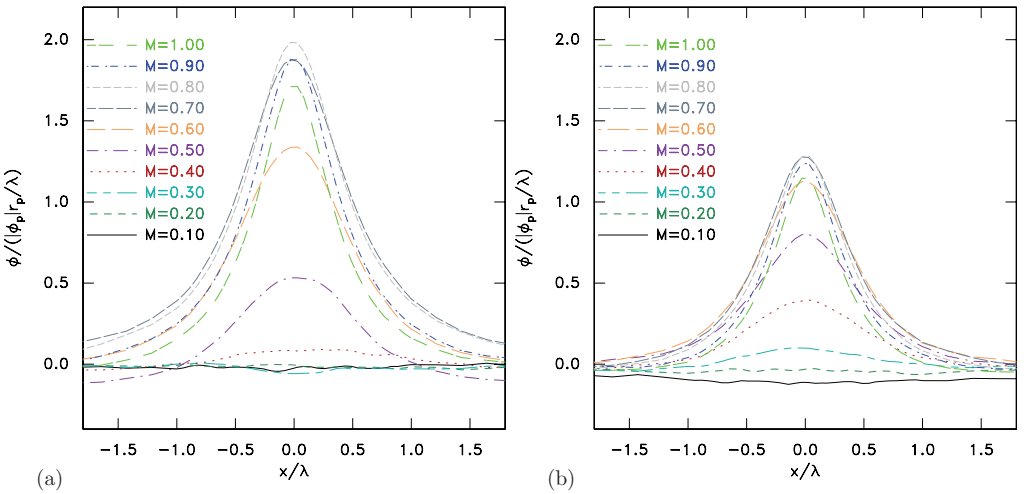

FIG. 4. (Color online) Wake transverse potential profile at $y = 0$, $z = 1$. (a) Collisionless plasma and (b) collisional plasma. In the nearly linear regime the point charge $\bar{Q} = -0.02$.

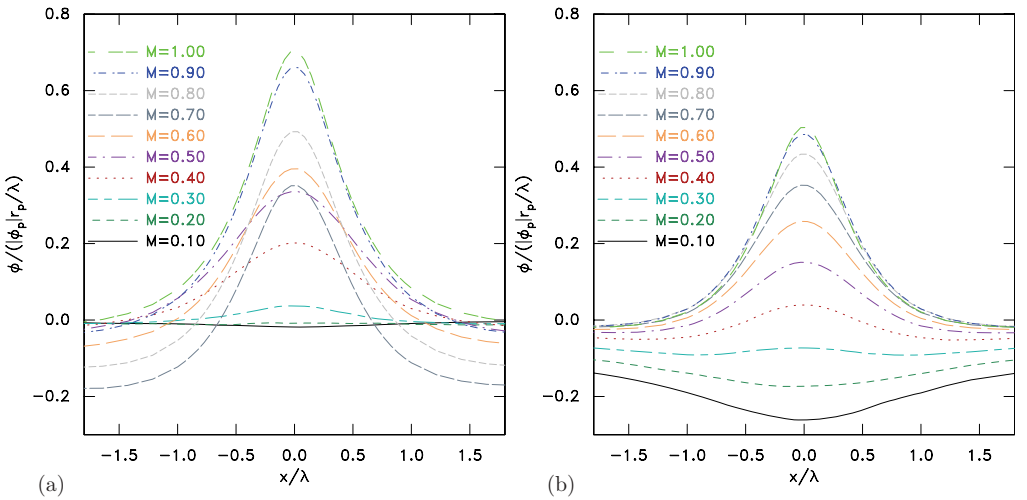

FIG. 5. (Color online) Wake transverse potential profile at $y = 0, z = 1$. (a) Collisionless plasma and (b) collisional plasma. In the nonlinear regime the point charge $\bar{Q} = -0.2$.

low M. Collisional trapping causes an enormous rise of the ion density in the grain's potential well: as much as a factor of 200. The physics is thus making a transition at low Mach number to the spherically symmetric collisional collection, with shielding dominated by ions, as studied in Refs. [25,31].

Summarizing the single-grain wake potential observations, for collisionless and collisional, nearly linear and nonlinear plasmas, at $T_e/T_i = 100$, the attractive wake potential peak disappears (or at least is greatly reduced) for flow Mach numbers of about 0.3 and below.

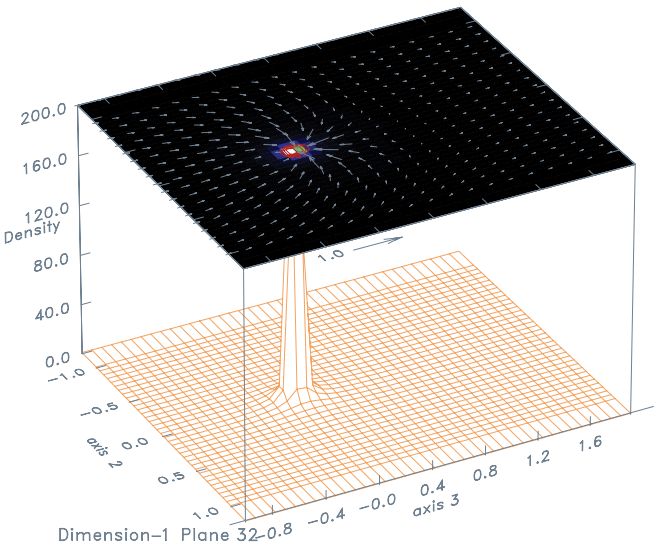

FIG. 6. (Color online) Flow pattern for the collisional case at low drift $M = 0.1$ (in direction of axis 3) in the vicinity of a large charge $\bar{Q} = -0.2$. Arrows indicate the magnitude and direction of the ion mean velocity in the plane $x =$ const through the origin. The ion velocity converges to compensate for the effective loss to the grain. The ion density (relative to ambient) in this plane is shown as a three-dimensional surface and contours. It becomes extremely large in the potential well because of trapped ions: as much as 200 times ambient.

IV. TWO-GRAIN SIMULATIONS

The full nonlinear calculation of the force on the downstream grain requires a three-dimensional calculation with two grains. One is at the origin and the second having the same charge for these calculations is placed at $z = 1, x = 0.5$, $y = 0$ (in units of λ_{De}). A comparison with Figs. 4 and 5 shows that this transverse position is near the maximum of the potential gradient, thus giving a representative measure of the transverse, grain-aligning, force.

Shown in Fig. 7 is the wake potential calculated by COPTIC on a domain of size $(\pm 4, \pm 4, -4 \to 8)\lambda_{De}$ spanned by a mesh $64 \times 64 \times 100$. The plasma drift velocity is in the z direction (along axis 3). The deep potential wells caused by the two charged grains are cut off conveniently for viewing. Immediately behind them are two potential peaks that are partly joined. For this $M = 0.6$ case, a combined oscillatory

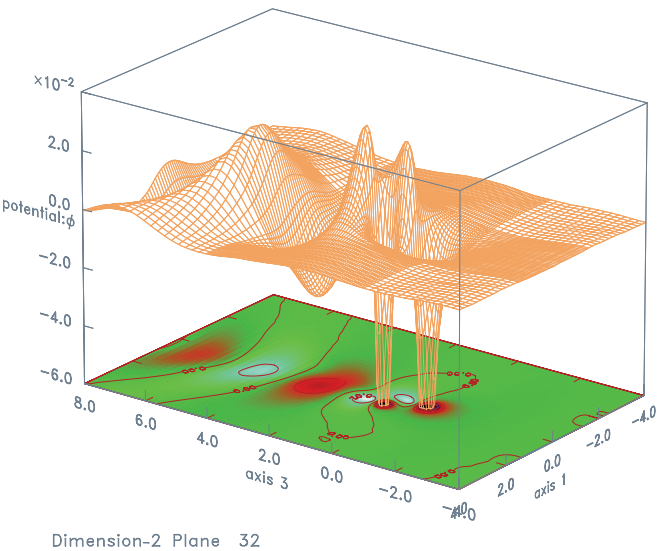

FIG. 7. (Color online) Wake potential for two grains at $M = 0.6$. The slice shown is on the plane $y = 0$. In the collisionless plasma, nearly linear regime the point charge $\bar{Q} = -0.02$.

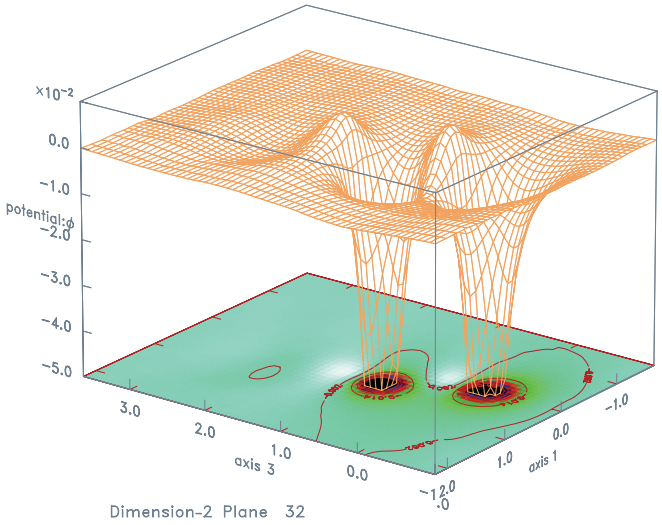

FIG. 8. (Color online) Wake potential for $M = 0.3$. The slice shown is on the plane $y = 0$. In the collisionless plasma, nearly linear regime the point charge $\bar{Q} = -0.02$.

wake is present beyond the two peaks, which does not look much different from a typical one-grain wake.

Figure 8 shows the case $M = 0.3$, where the oscillatory wake damps out very quickly. Therefore the plot is focused on the inner region. (The full simulation domain is the same as in Fig. 7 for all calculations in this paper.) The result shows only the vestiges of the trailing positive potential peaks and negligible oscillations. Figure 9 is for $M = 0.1$, where even those vestiges have disappeared and the only relevant remaining features are the two potential wells of the two grains.

A large number of simulation ions (about 100×10^6) in the code is required to obtain the *force* on the grains without excessive noise. Each Mach number requires a different simulation of course, each of which is a moderately expensive calculation (about 1 h of 128 processors for 1000 time steps).

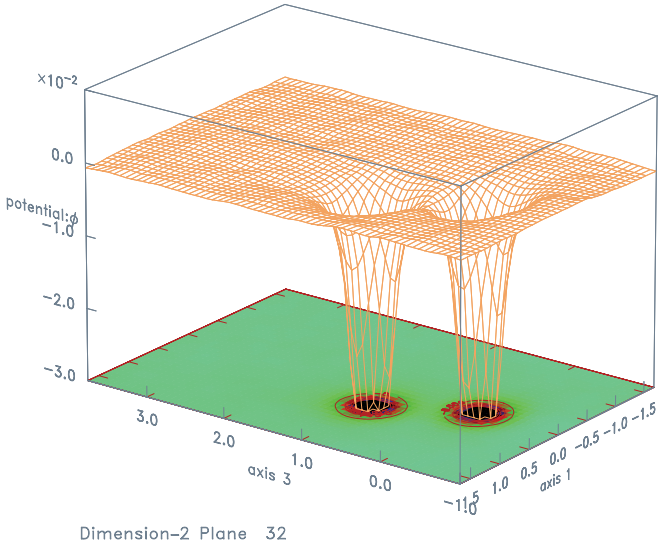

FIG. 9. (Color online) Wake potential for $M = 0.1$. The slice shown is on the plane $y = 0$. In the collisionless plasma, nearly linear regime the point charge $\bar{Q} = -0.02$.

The force on the downstream grain is measured in the code by integration of the total momentum flux across each of three different spheres (of radius $0.3\lambda_{De}$, $0.4\lambda_{De}$, and $0.5\lambda_{De}$) centered on the downstream grain. A perfect steady-state calculation ought to give the same total force for each of these spheres. In Fig. 10 these different measures are plotted to give an indication of the (rather small) uncertainty arising mostly from mesh resolution. The good reproducibility of the small forces was also documented by performing equivalent runs but for different choice of coordinates: $x = 0$, $y = 0.5$ or $x = -0.5$, $y = 0$, etc.

Collisionless results for the transverse force on the downstream grain are shown in Fig. 10 for two different grain-charge values. The attractive force, toward the z axis, is positive on the plot. In other words, the ordinate is minus the x force when the x position is positive. The two-grain simulation results (points) are compared with the force on the downstream grain that would arise from the transverse electric field that exists in the wake of the upstream grain alone (line). It has been shown previously that at sonic speeds the single-grain wake field force agrees quite well with the full two-grain force calculation. This agreement is observed here also at low Mach number. For a grain charge small enough to be in the nearly linear regime [Fig. 10(a)] the agreement is very good. In the nonlinear regime [Fig. 10(b)] it is not as good, especially in the transition region near $M = 0.4$. The two-grain calculation shows the force going abruptly to nearly zero, whereas the transverse wake field gradient reaches nearly zero only at a lower Mach number $M \sim 0.3$.

The transverse force on the *upstream* particle is found to be typically a factor of 5 smaller in magnitude than the force on the downstream particle. Moreover, it has the *same* sign, not the opposite sign one might expect for action and reaction if a direct interparticle force were involved. This observation is entirely consistent with the expectation that the upstream particle experiences mostly the shielded repulsive field of the downstream particle. It is the downstream attractive transverse force that is anomalous in its direction. It is attractive because of the wake effects. These observations emphasize the nonreciprocal nature of the particles' effective interaction, as mediated by the plasma. Of course, at zero flow velocity the situation becomes symmetric between upstream and downstream and their transverse forces must become equal and opposite. However, in all but the nonlinear collisional case studied here the forces have become too small to measure reliably in the code at the lowest velocity explored.

When neutral collisions are present, the transverse force on the downstream grain is modified as illustrated in Fig. 11. In the nearly linear charge-magnitude regime [Fig. 11(a)] there is still quite good agreement between the full two-grain simulation force and the single-grain wake field force. The overall magnitude of the force is suppressed by about 30% from the collisionless case and it approaches zero for $M \lesssim 0.35$. However, in the nonlinear case, there are major discrepancies between the actual transverse force and the wake field (i.e., between the points and the line). The collisions suppress the force at intermediate Mach numbers ($0.5 \leqslant M \leqslant 1$) much more than the single-grain wake field. At low Mach numbers the force remains attractive (positive

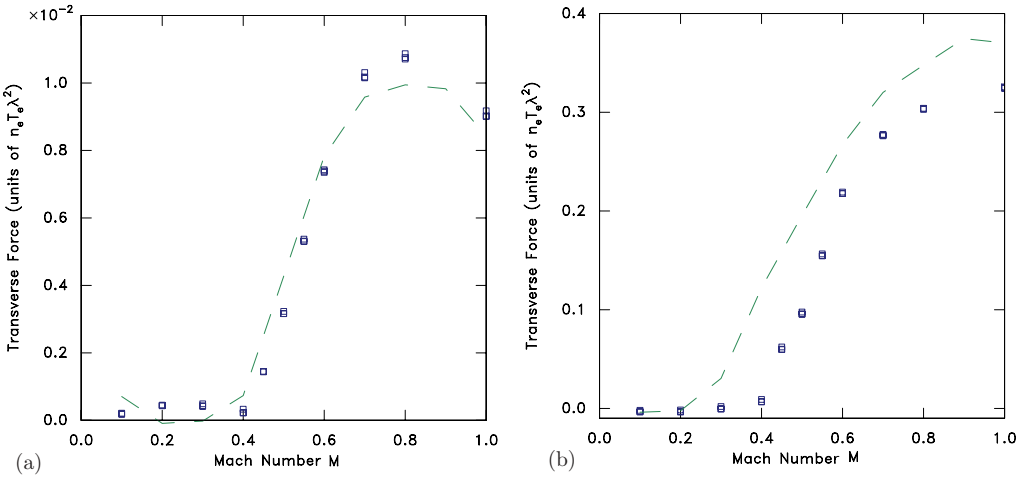

FIG. 10. (Color online) Transverse force in the collisionless plasma on an equal grain at downstream position $z = 1$, $x = 0.5$, $y = 0$ versus flow Mach number M. The points denote the two-grain simulation, total force and the dashed line is the gradient of the one-grain wake potential. (a) In the nearly linear regime the point charge $\bar{Q} = -0.02$ and (b) in the nonlinear regime the point charge $\bar{Q} = -0.2$.

on the plot here), whereas the wake field actually reverses in sign below $M = 0.3$. The force remains positive apparently because the ion drag perturbation on the downstream particle becomes more important than the potential gradient. The convergence of the transverse velocity, illustrated in Fig. 6, then overcomes the electric repulsion of Fig. 5(b). We cannot rule out, however, that there are other synergistic two-particle effects that contribute.

The attractive force remaining positive at low velocity might have significance for the experiments that observe grain alignment even at low flow velocity [22]. Figure 11(b) shows a nonzero attractive (transversely aligning) force in the nonlinear collisional case even at $M = 0.1$. The force is quite a small fraction (perhaps 10%) of the aligning force at $M = 1$, but might be large enough to be significant. The magnitude of charge in this case is approximately what would be acquired by a grain of radius $0.1\lambda_{\mathrm{De}}$, which is probably rather larger than most experiments. Ten times smaller grains [Fig. 11(a)] appear to have little residual attraction at low M.

V. CONCLUSION

It has been shown that the oscillations in the wake of a small charged grain disappear because of damping: either collisional damping when the flow velocity is large or Landau damping when the flow velocity is reduced below a few times the ion thermal velocity. However, neutral collisions sufficient to remove oscillations do not of themselves remove the ion density enhancement immediately behind a negatively charged grain, caused by focusing. Extensive computations show that the wake density enhancement and the related potential peak disappear quite abruptly as the flow velocity is reduced below approximately $0.3c_s$ (for $T_e/T_i = 100$). This disappearance causes the transverse, grain-aligning force on a grain in the wake of another to become negligible. The

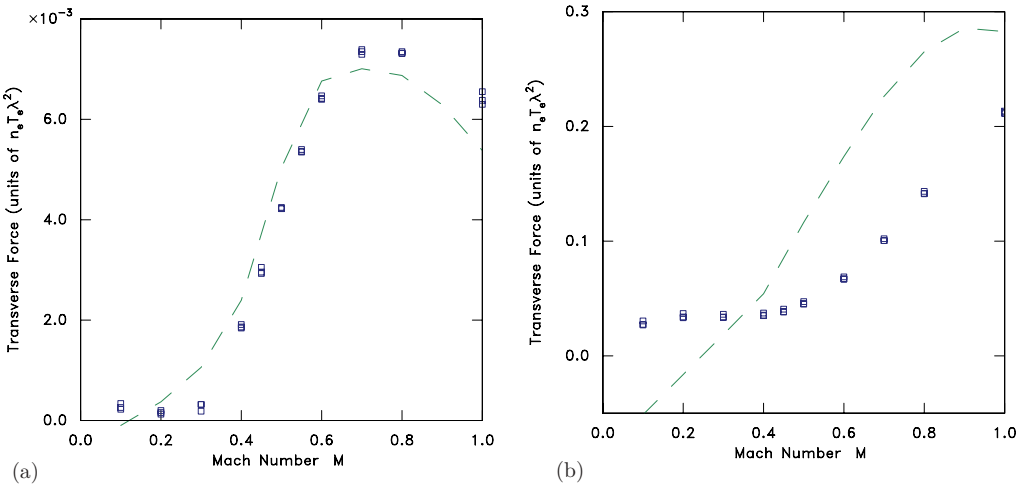

FIG. 11. (Color online) Transverse force in collisional plasma on an equal grain at downstream position $z = 1$, $x = 0.5$, $y = 0$ versus flow Mach number M. The points denote the two-grain simulation, total force and the dashed line is the gradient of the one-grain wake potential. (a) In the nearly linear regime the point charge $\bar{Q} = -0.02$ and (b) in the nonlinear regime the point charge $\bar{Q} = -0.2$.

two-grain three-dimensional computations confirm that for collisionless plasmas the tranverse force is well represented by the gradient of the single-grain wake potential for small grains even at low Mach numbers in the nearly linear regime. It is somewhat less well represented in the nonlinear regime. For collisional plasmas in the nonlinear regime the wake potential gradient does not represent the transverse force well and a small residual grain-aligning force (about one-tenth of the force for sonic flows) remains at Mach numbers down to 0.1. Although the presence of this residual force does not allow one to immediately rule out an explanation of grain alignment and chains at low Mach numbers, its smallness, as well as its absence in the nearly linear regime, suggests that other mechanisms, omitted from the present calculations, ought to be considered. These might include forces arising from direct neutral gas effects on the grain: drag or thermophoretic forces. They might also include the collective effects of the other nearby grains.

ACKNOWLEDGMENTS

I am grateful to Christian Bernt Haakonsen for illuminating conversations and to Patrick Ludwig for related collaboration. This work was partially supported by the National Science Foundation–Department of Energy Grant No. DE-FG02-06ER54982.

[1] J. S. Halekas, V. Angelopoulos, D. G. Sibeck, K. K. Khurana, C. T. Russell, G. T. Delory, W. M. Farrell, J. P. McFadden, J. W. Bonnell, D. Larson, R. E. Ergun, F. Plaschke, and K. H. Glassmeier, Space Sci. Rev. **165**, 93 (2011).
[2] R. E. Ergun, D. M. Malaspina, S. D. Bale, J. P. McFadden, D. E. Larson, F. S. Mozer, N. Meyer-Vernet, M. Maksimovic, P. J. Kellogg, and J. R. Wygant, Phys. Plasmas **17**, 072903 (2010).
[3] I. H. Hutchinson, Phys. Plasmas **15**, 123503 (2008).
[4] I. H. Hutchinson and L. Patacchini, Plasma Phys. Controlled Fusion **52**, 124005 (2010).
[5] J. H. Chu and L. I, Phys. Rev. Lett. **72**, 4009 (1994).
[6] A. Melzer, V. A. Schweigert, I. V. Schweigert, A. Homann, S. Peters, and A. Piel, Phys. Rev. E **54**, R46 (1996).
[7] K. Takahashi, T. Oishi, K.-i. Shimomai, Y. Hayashi, and S. Nishino, Phys. Rev. E **58**, 7805 (1998).
[8] A. Melzer, V. A. Schweigert, and A. Piel, Phys. Rev. Lett. **83**, 3194 (1999).
[9] V. Steinberg, R. Sütterlin, A. V. Ivlev, and G. Morfill, Phys. Rev. Lett. **86**, 4540 (2001).
[10] G. A. Hebner and M. E. Riley, Phys. Rev. E **68**, 046401 (2003).
[11] G. A. Hebner and M. E. Riley, Phys. Rev. E **69**, 026405 (2004).
[12] M. Kroll, J. Schablinski, D. Block, and A. Piel, Phys. Plasmas **17**, 013702 (2010).
[13] N. Rostoker, Nucl. Fusion **1**, 101 (1961).
[14] J. Sanmartin and S. Lam, Phys. Fluids **14**, 62 (1971).
[15] L. Chen, A. Langdon, and M. Lieberman, J. Plasma Phys. **9**, 311 (1973).
[16] M. Lampe, G. Joyce, G. Ganguli, and V. Gavrishchaka, Phys. Plasmas **7**, 3851 (2000).
[17] P. C. Stangeby and J. E. Allen, J. Plasma Phys. **6**, 19 (1971).
[18] F. Melandso and J. Goree, Phys. Rev. E **52**, 5312 (1995).
[19] I. H. Hutchinson, Phys. Plasmas **18**, 032111 (2011).
[20] I. H. Hutchinson, Phys. Rev. Lett. **107**, 095001 (2011).
[21] B. Annaratone, S. Khrapak, P. Bryant, G. Morfill, H. Rothermel, H. Thomas, M. Zuzic, V. Fortov, V. Molotkov, A. Nefedov, S. Krikalev, and Y. Semenov, Phys. Rev. E **66**, 056411 (2002).
[22] O. Arp, J. Goree, and A. Piel, Phys. Rev. E **85**, 046409 (2012).
[23] I. H. Hutchinson, arXiv:1105.1356.
[24] R. W. Hockney and J. W. Eastwood, *Computer Simulation using Particles* (Taylor and Francis, London, 1988).
[25] I. H. Hutchinson and L. Patacchini, Phys. Plasmas **14**, 013505 (2007).
[26] C. K. Birdsall and A. B. Langdon, *Plasma Physics via Computer Simulation* (IOP, Bristol, 1991), p. 20ff.
[27] L. Patacchini and I. H. Hutchinson, Phys. Rev. Lett. **101**, 025001 (2008).
[28] D. Winske, W. Daughton, D. Lemons, and M. Murillo, Phys. Plasmas **7**, 2320 (2000).
[29] W. J. Miloch, Plasma Phys. Controlled Fusion **52**, 124004 (2010).
[30] P. Ludwig, W. J. Miloch, H. Kählert, and M. Bonitz (unpublished).
[31] M. Lampe, R. Goswami, Z. Sternovsky, S. Robertson, V. Gavrishchaka, G. Ganguli, and G. Joyce, Phys. Plasmas **10**, 1500 (2003).